BNL- 52493

UC-414

DIVERSE TOPICS IN CRYSTALLINE BEAMS

JIE WEI,
ANDREW DRAWSEKE AND ANDREW M. SESSLER (LBL),
XIAO-PING LI (BIOSYM TECHNOLOGIES)

NOVEMBER 27, 1995

RHIC PROJECT

Brookhaven National Laboratory
Associated Universities, Inc.
Upton, NY 11973

Under Contract No. DE-AC02-76CH00016 with the

UNITED STATES DEPARTMENT OF ENERGY

MASTER

DISTRIBUTION OF THIS DOCUMENT IS UNLIMITED

DISCLAIMER

This report was prepared as an account of work sponsored by an agency of the United States Government. Neither the United States Government nor any agency thereof, nor any of their employees, not any of their contractors, subcontractors, or their employees, makes any warranty, express or implied, or assumes any legal liability or responsibility for the accuracy, completeness, or usefulness of any information, apparatus, product, or process disclosed, or represents that its use would not infringe privately owned rights. Reference herein to any specific commercial product, process, or service by trade name, trademark, manufacturer, or otherwise, does not necessarily constitute or imply its endorsement, recommendation, or favoring by the United States Government or any agency, contractor, or subcontractor thereof. The views and opinions of authors expressed herein do not necessarily state or reflect those of the United States Government or any agency, contractor or subcontractor thereof.

Printed in the United States of America
Available from
National Technical Information Service
U.S. Department of Commerce
5285 Port Royal Road
Springfield, VA 22161

NTIS price codes:
Printed Copy: A06; Microfiche Copy: A01

DIVERSE TOPICS IN CRYSTALLINE BEAMS*

JIE WEI
Brookhaven National Laboratory, Upton, New York 11973
ANDREW DRAESEKE and ANDREW M. SESSLER
Lawrence Berkeley Laboratory, 1 Cyclotron Road, Berkeley, California 94720
XIAO-PING LI
BIOSYM Technologies Inc., 9685 Scranton Rd., San Diego, CA 92121

ABSTRACT

Equations of motion are presented, appropriate to interacting charged particles of diverse charge and mass, subject to the external forces produced by various kinds of magnetic fields and radio-frequency (rf) electric fields in storage rings. These equations are employed in the molecular dynamics simulations to study the properties of crystalline beams. The two necessary conditions for the formation and maintenance of crystalline beams are summarized. The transition from 1D to 2D, and from 2D to 3D is explored, and the scaling behavior of the heating rates is discussed especially in the high temperature limit. The effectiveness of various cooling techniques in achieving crystalline states has been investigated. Crystalline beams made of two different species of ions via sympathetic cooling are presented, as well as circulating "crystal balls" bunched in all directions by magnetic focusing and rf field. By numerically reconstructing the original experimental conditions of the NAP-M ring, it is found that only at extremely low beam intensities, outside of the range of the original measurement, proton particles can form occasionally-passing disks. The proposed New ASTRID ring is shown to be suitable for the formation and maintenance of crystalline beams of all dimensions.

1. Introduction

In previous work, the nature of crystalline beams has been studied by many different investigators.[1]–[15] In particular, we have made a systematic study in a series of papers[16]–[22] which has consisted of deriving the equations of motion for charged particles undergoing Coulomb interaction in a real storage ring, and then using them to study many properties of crystalline beams. We have shown that the storage ring must be alternating-gradient (AG) focusing, that operation must be below the transition energy of the ring, and that the storage ring lattice periodicity must be much greater than twice the maximum betatron (transverse) tune.

In this paper, we carry on our studies with investigations of a number of disparate crystalline beam subjects. First, we present in Section 2 the generalized equations

*Work performed under the auspice of the U.S. Department of Energy, supported by NSF Grant DMR-91-15342, and by the DOE, Office of Energy Research, Office of High Energy and Nuclear Physics, under Contract No.DE-AC03-76SF00098.

of motion appropriate to the study. Previously, we have presented a rather lengthy derivation[16] which considered one species of ions with no longitudinal external force; since the generalization is straight-forward, we only present the results. Using these equations, we then discuss in Section 3 some results of the molecular dynamics (MD) simulations including the method of determining the ground state, the evaluation of the heating rates, and the scaling laws in comparison with that obtained from the intra-beam scattering (IBS) theory.

In Section 4, we re-state the conditions for crystallization, emphasizing the second condition pertaining to the machine lattice periodicity and the maximum transverse tune. The phonon spectrum, which is the key to this condition, is investigated analytically for one-dimensional (1D), and numerically for 2D and 3D crystalline structures.

Previously, we achieved crystalline states in the MD simulation by imposing once per lattice period a condition of periodicity while correcting the longitudinal slippage.[16] To investigate the effectiveness of conventional cooling methods, we employ in Section 5 more realistic models of conventional stochastic, electron, and laser cooling, as well as the proposed longitudinally tapered cooling.

In Section 6, we study the development of crystalline beams consisting of two different ion species of similar rigidity, while only one species of which is subject to cooling. We show that sympathetic cooling due to intra-particle interaction cools the other species, resulting in crystalline structures of two types of ions. These structures possess more complicated properties than single-species structures.

To extend our knowledge into bunched beams, we further investigate in Section 7 the effect of a radio-frequency (rf) electric field upon the formation of 3D bunched "crystalline balls" circulating in the storage ring. Such "blobs of matter" should have interesting properties and applications different from that of usual crystalline beams which are finite only in the transverse directions.

In the late 1970's, anomalous behavior in the Schottky signals was observed on the NAP-M ring, leading to the suggestion of crystalline beams and precipitating a great deal of theoretical and experimental work. It is thus interesting to use the tools that we have developed to reconstruct the original conditions of the NAP-M ring, and to see whether, theoretically, a crystalline state could have been realized. The results are summarized in Section 8.

In Section 9, we apply the methodology to a ring which has been proposed for the careful study of crystalline beams; namely the New ASTRID ring. We determine the conditions under which 1D, 2D, and 3D crystalline structures can be formed, and determine the cooling rate needed for crystallization.

Finally, the conclusions are presented in Section 10.

2. Equations of Motion

In order to adopt the molecular dynamics (MD) methods, we employ[16] a rotating frame (x, y, z, t) of a reference particle in which the orientation of the axes is rotating so that the axes are constantly aligned to the radial (x), vertical (y), and tangential (z) direction of motion. The equations previously derived for the motion of the particles in the presence of bending dipole and focusing quadrupole magnetic fields, can be

generalized for multi-species of ions under various external dipole, quadrupole, and sextupole magnetic fields and longitudinal electric fields.

It is convenient to define a reference particle with charge state Z_0 and atomic mass M_0. We scale dimensions in terms of the characteristic distance ξ, with $\xi^3 = r_0\rho^2/\beta^2\gamma^2$, where $r_0 = Z_0^2e^2/M_0c^2$, the velocity of the reference particle is βc, its energy is γM_0c^2, and it moves on an orbit with bending radius ρ in magnetic field B_0. We measure time in units of $\rho/\beta\gamma c$ and energy in units of $\beta^2\gamma^2 Z_0^2e^2/\xi$. For the ith species of ions with electric charge state Z_i and mass M_i, we define the relative charge and mass with respect to the reference values

$$\bar{Z}_i \equiv Z_i/Z_0, \quad \text{and} \quad m_i \equiv M_i/M_0. \tag{1}$$

In a bending region with bending radius ρ, the equations of motion for particles of the ith species can be derived as

$$\begin{cases} \ddot{x} - \left(2 - \dfrac{\bar{Z}_i}{m_i}\right)\gamma\dot{z} + \left[1 - \left(2 - \dfrac{\bar{Z}_i}{m_i}\right)\gamma^2\right]x + \left(\dfrac{\bar{Z}_i}{m_i} - 1\right)\dfrac{\rho}{\xi} &= -\dfrac{\partial V_{Ci}}{\partial x}, \\ \ddot{y} &= -\dfrac{\partial V_{Ci}}{\partial y}, \\ \ddot{z} + \left(2 - \dfrac{\bar{Z}_i}{m_i}\right)\gamma\dot{x} + \left(\dfrac{\bar{Z}_i}{m_i} - 1\right)\gamma^2 z &= -\dfrac{\partial V_{Ci}}{\partial z}, \end{cases} \tag{2}$$

where the dots denote differentiations with respect to the time t measured in the above units, the Coulomb potential is

$$V_{Ci}(x,y,z) = \sum_j \frac{\bar{Z}_i\bar{Z}_j}{m_i\sqrt{(x_j-x)^2 + (y_j-y)^2 + (z_j-z)^2}}, \tag{3}$$

and the summation, j, is over all the other particles. The Hamiltonian that corresponds to Eqs. 2 and 3 is

$$\begin{aligned} H_i(x,P_x,y,P_y,z,P_z;t) &= \frac{1}{2}\left(P_x^2 + P_y^2 + P_z^2\right) + \frac{1}{2}\left[x^2 + \left(\frac{\bar{Z}_i}{m_i} - 1\right)\gamma^2 z^2\right] \\ &\quad - \left(2 - \frac{\bar{Z}_i}{m_i}\right)\gamma x P_z + \left(\frac{\bar{Z}_i}{m_i} - 1\right)\frac{\rho}{\xi}\,x + V_{Ci}(x,y,z). \end{aligned} \tag{4}$$

In a straight section, where there is no bending of particles, there often are quadrupole magnets for focusing, sextupole magnets for chromatic correction, and electric field for acceleration or bunching. If the quadrupole and sextupole strengths are represented by

$$n_1 = -\frac{\rho}{B_0}\frac{\partial B_y}{\partial x} \quad \text{and} \quad n_2 = -\frac{\rho}{B_0}\frac{\partial^2 B_y}{\partial x^2}, \tag{5}$$

respectively, the equations of motion can be derived as

$$\begin{cases} \ddot{x} - \dfrac{\bar{Z}_i}{m_i}\left[n_1 x + \dfrac{n_2\xi}{2}(x^2 - y^2)\right] &= -\dfrac{\partial V_{Ci}}{\partial x}, \\ \ddot{y} + \dfrac{\bar{Z}_i}{m_i}(n_1 y + n_2\xi xy) &= -\dfrac{\partial V_{Ci}}{\partial y}, \\ \ddot{z} &= -\dfrac{\partial V_{Ci}}{\partial z} + F_s, \end{cases} \tag{6}$$

where the electrical force F_s in the reduced units can be expressed in terms of electric field E_s measured in the laboratory frame,

$$F_s \equiv -\frac{\partial U_s}{\partial z} = \frac{\bar{Z}_i}{m_i}\frac{Z_0 e E_s \xi}{M_0 c^2}\left(\frac{\rho}{\xi\beta\gamma}\right)^2. \tag{7}$$

The corresponding Hamiltonian is

$$\begin{aligned} H_i(x, P_x, y, P_y, z, P_z; t) &= \frac{1}{2}\left(P_x^2 + P_y^2 + P_z^2\right) - \frac{n_1}{2}\frac{\bar{Z}_i}{m_i}(x^2 - y^2) \\ &\quad -\frac{n_2\xi}{6}\frac{\bar{Z}_i}{m_i}(x^3 - 3xy^2) + V_{Ci}(x, y, z) + U_s. \end{aligned} \tag{8}$$

In the reduced units, the revolution period of the reference particle in the storage ring is C_0/ρ, where $C_0 = 2\pi R$ is the circumference of the ring.

Obviously, in the case that only one species of ions is studied, $\bar{Z}_i = m_i = 1$, Eqs. 2 – 8 become much simplified.

3. Molecular Dynamics Results

In previous papers, we have presented many computational results which the reader may wish to consult. In this section, we present results from several different MD studies of single-species un-bunched beam, emphasizing the method of determining the ground states, the scaling behavior of the heating rates, and the comparison with the IBS theory.

3.1 A Study of 1D to 2D, and 2D to 3D Transitions

It has been well established[7] that at very low line density (beam intensity), a crystalline beam is a 1D string. As the density is increased beyond critical values, the ground state first converts from 1D into 2D extending in the plane of weaker focusing, then from 2D into 3D. As the density is increased even further, the structure expands in transverse dimension, while the intra-particle distance remains approximately the same.

In order to determine the ground state at a given density and to study the transition from 1D to 2D, and from 2D to 3D, we have undertaken extensive numerical

computations. For simplicity but without losing generality, we present an example using a constant gradient (CG) harmonic oscillator model, instead of an AG focusing ring, with the transverse focusing strengths $K_x = 2.8$ and $K_y = 3.2$. Fig. 1 shows

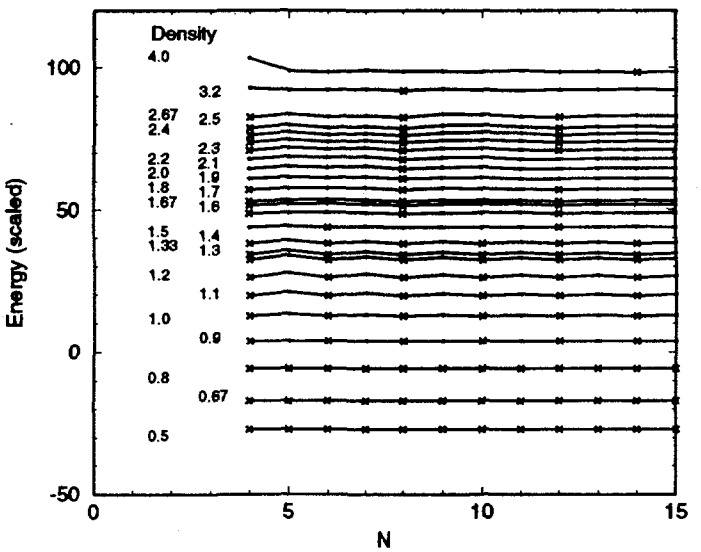

Figure 1: Lowest energies achievable with a finite number of particles N per MD cell of length L in the MD calculations at various densities N/L. The crosses show the lowest energy achievable at the particular density.

the lowest energies achievable with a finite number of particles N per MD cell of length L in the MD calculations at various densities N/L (The vertical axis shows scaled energy obtained by the expression $15N/L + 100E$, where E is the sum of the average kinetic and potential energy of the particles, and L is in units of ξ.). When $N/L \leq 0.8$, the ground state is a 1D chain of equally spaced particles, which can be obtained with any number of test particles per MD cell, as shown by the crosses in Fig. 1. Within the range $0.9 \leq N/L \leq 1.4$, the ground state is a 2D zig-zag, which can be obtained only with even number of test particles per MD cell, again as shown by the crosses in Fig. 1. When $N/L \geq 1.5$, the ground state becomes 3D. The minimum number of test particles needed to achieve the lowest-energy state increases. For example, the lowest energy state for the $N/L = 2$ case can be obtained only when the number of test particles is an integral multiple of 8. Fig. 2 shows a 3D view of such a double-helix structure.

3.2 Temperatures and Heating Rates

For the time dependent Hamiltonian system discussed in Section 2, it is advantageous to define the normalized beam temperature in terms of the deviation of P_x, P_y

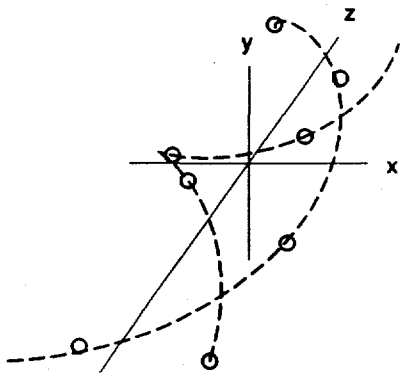

Figure 2: A 3D view of a 3D double-helix structure at $N/L = 2$ in a constant-gradient potential. In this study, the transverse focusing strengths are $K_x = 2.8$ and $K_y = 3.2$.

and P_z from their ground-state values,

$$T_x = \langle(\Delta P_x)^2\rangle, \quad T_y = \langle(\Delta P_y)^2\rangle, \quad \text{and} \quad T_z = \langle(\Delta P_z)^2\rangle, \tag{9}$$

squared and averaged both over different particles and over a time period (typically 20 lattice periods) that is long compared with the focusing period but short compared with the total time of observation. When the system temperature is sufficiently higher than the break-up temperature (transition between crystalline and "running" state[20]) of the crystalline state,[20] the normalized temperature T can be directly related to the conventionally used beam temperature T_B, un-normalized rms beam emittance $\epsilon_{x,y}$, and rms momentum spread $\Delta p/p$ by the relations

$$\frac{\xi^2}{\rho^2}[T_x, T_y, T_z] \approx \frac{2k_B}{\beta^2\gamma^2 M_0 c^2}[T_{Bx}, T_{By}, T_{Bz}] = \left[\frac{\epsilon_x}{\bar{\beta}_x}, \frac{\epsilon_y}{\bar{\beta}_y}, \frac{1}{\gamma^2}\left(\frac{\Delta p}{p}\right)^2\right], \tag{10}$$

where k_B is the Boltzmann constant, and $\bar{\beta}_{x,y}$ are the average amplitude functions of the machine lattice. When the system temperature in one or more direction is lower than the break-up temperature, the conventionally used quantities T_B, $\epsilon_{x,y}$, and $\Delta p/p$ can not properly characterize the ordered state.

In a typical storage ring, the particles under Coulomb interaction absorb energy from the AG lattice via a multi-phonon process.[22] In the absence of cooling, Fig. 3 shows the rate of temperature increase (heating rate) as a function of temperature at various beam densities that correspond to 1D ($N/L = 0.25$), single-shell 3D ($N/L = 1$), and multi-shell 3D ($N/L = 25$) ground states. The machine consists of 10 FODO cells with 25% bending with $\nu_x = 2.8$, $\nu_y = 2.1$, and the beam energy is $\gamma = 1.4$. It is

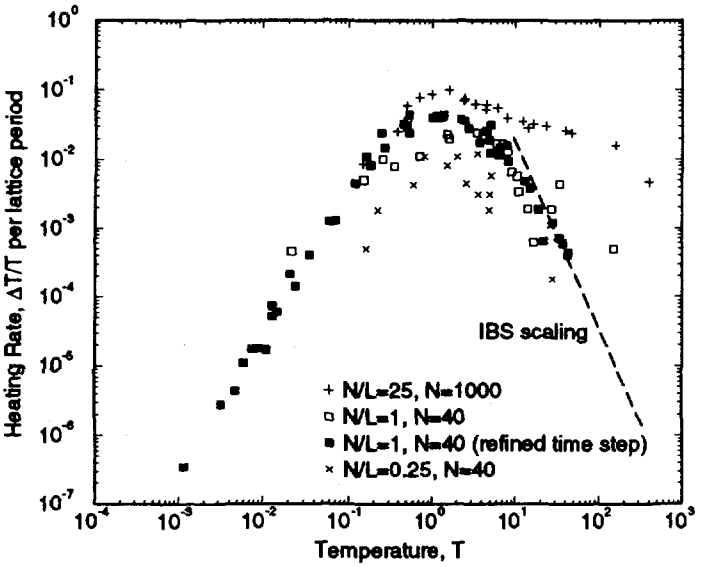

Figure 3: Heating rates as functions of temperature at various beam densities N/L. Here, N is the number of particles per MD cell of length L in units of ξ.

observed that the break-up temperature $T \approx 1$ corresponds to the peak heating rate, independent of the beam density. On the other hand, the peak heating rate increases with the beam density. Typically, strong correlation in particle position appears in all directions when the temperature is below $T \approx 0.05$.

At low temperature, the heating rate is low. Numerically, a large number of iteration steps is required to accumulate a noticeable amount of temperature increase. On the other hand, at high temperature the particle velocity is high. In both low and high temperature range, we often need refined iteration step size and increased number N of particles per MD cell to achieve high numerical accuracy. The comparison between different step sizes is shown by the filled and empty squares in Fig. 3.

3.3 High Temperature Limit

At temperatures high compared with that for the formation of crystalline structure, intra-beam Columb scattering (IBS) theory can be readily used to describe the beam heating. We expresses the heating rate in terms of the growth rate of the beam

temperature T_B as

$$\begin{bmatrix} \frac{1}{T_{Bz}}\frac{dT_{Bz}}{dt} \\ \frac{1}{T_{Bx}}\frac{dT_{Bx}}{dt} \\ \frac{1}{T_{By}}\frac{dT_{By}}{dt} \end{bmatrix} = \frac{Z^4 N_0 r_0^2 L_c \beta^2 c}{2^{3/2} A^2 \bar{\beta}_x \bar{\beta}_y C_0 T_{Bx} T_{By} T_{Bz}^{1/2}} \left(\frac{M_0 c^2}{2k_B}\right)^{5/2} F\left(\frac{a^2+b^2}{2}\right) \begin{bmatrix} 2(1-d^2) \\ -\frac{a^2}{2}+d^2 \\ -\frac{b^2}{2} \end{bmatrix}, \tag{11}$$

where

$$d^2 \approx \frac{\gamma^2 T_{Bz}}{\gamma_T^2 T_{Bx} + \gamma^2 T_{Bz}},\ a^2 \approx \frac{\gamma_T^2}{\gamma^2} d^2,\ b \approx \frac{T_{Bx}}{T_{By}} d^2, \tag{12}$$

$F(\ )$ is a "form factor" (Ref. [23]), L_c is the Coulomb logarithm, N_0 is the total number of particles in the storage ring of circumference C_0, γ_T is the relativistic factor of the transition energy, and A is the atomic mass number. Ignoring the dependence on the detailed beam configuration, the heating rate can be rewritten in terms of the normalized temperature T as

$$\frac{1}{T}\frac{dT}{dt} \sim \frac{N}{L} \frac{\beta c L_c \rho}{2\pi^{1/2} \bar{\beta}_x \bar{\beta}_y T_x T_y T_z^{1/2}}, \tag{13}$$

where $N/L \equiv N_0 \xi / C_0 \gamma$ is the number of particles per unit length in units of ξ. The heating rate at high temperature is shown to be linearly proportional to the number of particles N_0 (or linear density N/L) of the beam. When the temperature increases, the rate decreases proportionally with $T^{5/2}$. Furthermore, the rate is linearly proportional to the beam velocity βc, similar to the way that conventional cooling rate behaves.

The results from the MD simulation can be readily compared with the IBS theory. In this temperature regime, we choose the MD time step so that the particle displacement in one time step is much smaller than the typical intra-particle distance. The heating rate is evaluated as a function of the beam temperature for density $N/L = 1$. As shown in Fig. 3, the temperature dependence of the heating rate obtained from the MD simulation (filled squares) agrees well with that obtained from the IBS theory (dashed line). On the other hand, the MD results completely disagree with the IBS extrapolation at the low temperature regime.

4. Conditions for Crystallization

In previous works, we have derived two conditions which are necessary to form and maintain the crystalline beams. Since the present storage rings do not satisfy these conditions, there is considerable interest in designing and building rings suitable for the study of crystalline beams. In view of this fact, we present once again these conditions with more detailed discussion.

4.1 First Condition

The first condition requires that the ring is alternating-gradient focusing, as contrasted to constant-gradient focusing. In addition, it is required that the energy of

the particles is less than the transition energy, i.e.

$$\gamma < \gamma_T. \tag{14}$$

In a typical ring, γ_T is approximately equal to the horizontal tune ν_x (number of betatron oscillation wavelengths in a circumference).

4.2 Second Condition

The second condition arises from the requirement that there is no linear resonance between the phonon modes of the crystalline structure and the machine lattice periodicity. Note that this is a condition for the maintenance of a crystalline beam, in contrast to the first condition which is for the formation of a crystalline beam.

In 1D case, the phonon spectrum can be analytically derived in the smooth approximation.[22] Typically, the highest phonon frequency is close to the maximum betatron tune. In order for the beam to avoid the linear resonance produced by the periodic modulation of the machine AG lattice, the lattice periodicity ω_l should be at least twice as high as the maximum betatron tune $\max(\nu_x, \nu_y)$.

For 3D crystalline structures having many shells, the phonon spectrum may be found approximately by ignoring the detailed structure and considering the properties of a uniformly charged rod. The frequency of the monopole mode, which is likely to be the highest frequency of the beam, has been previously derived[24] to be $\sqrt{2}\nu_{x,y}$. Thus, in the high density limit, the second condition becomes

$$2\sqrt{2}\ \max(\nu_x, \nu_y) < \omega_l. \tag{15}$$

At intermediate densities, the phonon modes can no longer be found analytically. In this case, we first employ the molecular dynamics to determine the ground-state structures. Then, using a newly written computer program, we calculate the phonon spectrum in smooth approximation (The detailed description of the method and results will be published elsewhere.). It has been verified that the highest phonon frequency is always less than $\sqrt{2}\max(\nu_x, \nu_y)$.

Therefore, in order to maintain crystalline beams at any beam density, the storage ring should be designed such that the lattice periodicity is at least $2\sqrt{2}$ as high as the maximum betatron frequency tune (Eq. 15).

5. Study of Cooling Methods

In finding the ground state in most of our early numerical simulations, we "cool" once per lattice period by simply imposing a condition of periodicity (by averaging initial and final coordinates and momenta) while correcting P_z according to the amount of slippage in z for each particle. Imposing the periodicity condition is a fast and effective way of finding a periodic or ground state. However, it is experimentally unrealistic at least at the current stage of technology. Therefore, we made numerical models that describe the actual experimental cooling. Our work, quite clearly, sheds light upon the subject of what experimental cooling methods are effective for the crystalline formation.

5.1 Model for Stochastic, Electron, and Laser Cooling

We simulate the actual cooling by reducing once per lattice period the momentum component P_i of each particle by a certain fraction,

$$\Delta P_i = -f_i P_i, \quad i = x, y, z. \tag{16}$$

By observing the reduction of temperature as a function of time, we determine the effectiveness of cooling when f_x, f_y, and f_z are varied.

When the beam density is low such that the ground state is a 1D chain, the ground state can be achieved by cooling in three directions with a rate higher than the maximum heating rate (Numerically, the cooling time is often several orders of magnitude slower than by imposing the periodicity condition). If cooling is only applied to the longitudinal direction (similar to regular laser cooling), the longitudinal temperature can be greatly reduced. Not surprisingly, the transverse temperature often can not be effectively reduced in this case for lack of sufficient IBS interaction.

When the beam density is high so that the ground state is 2D or 3D extending in the radial direction, all particles must have the same average angular velocity and, therefore, have different average linear velocity. Typically, there is no place in the ring lattice where all the particles have the same linear velocity in the ground state. Therefore, cooling in only the longitudinal direction ($f_x = f_y = 0$) often fails to produce a periodic crystalline state. On the other hand, cooling in the transverse direction is very effective for attaining a periodic crystalline state.

As an example, we study the case of a single-shell ground state ($N/L = 1$) in Fig. 3 with the machine consisting of 10 FODO cells with 25% bending with $\nu_x = 2.8$, $\nu_y = 2.1$, and $\gamma = 1.4$. When cooling is applied only in the longitudinal direction ($f_x = f_y = 0$), temperatures in all directions can be greatly reduced (often to $T \leq 0.1$) through IBS interaction reaching an intermediate non-gaseous state, as shown in Fig. 4 along the $f_x = f_y = 0$ axis with $f_z \geq 0.03$. However, since further reduction in temperature can not be achieved (except for the $f_z = 0.03$ case), ordering in the beam can not be realized.

When cooling is applied to the transverse direction ($f_z = 0$), temperature in all directions can be greatly reduced. Ordering in the beam can be achieved when the cooling strength is in the range $0.04 < f_{x,y} < 0.45$. After the ordering is achieved, the same ground state as given by imposing the periodicity condition can be achieved when the actual transverse cooling is adiabatically turned off. On the other hand, rapid actual cooling in the longitudinal direction ($f_z > 0.06$) almost always destroys ordering.

The implication of these studies is that the present cooling techniques suffice in making 1D crystals. In order to make higher density structures, it is necessary to develop cooling methods that are effective in the transverse as well as the longitudinal direction.

5.2 Model for Tapered Cooling

At the crystalline ground state, the radial displacement of the particle is linearly proportional to the particle momentum P_z. Therefore, an alternative method of

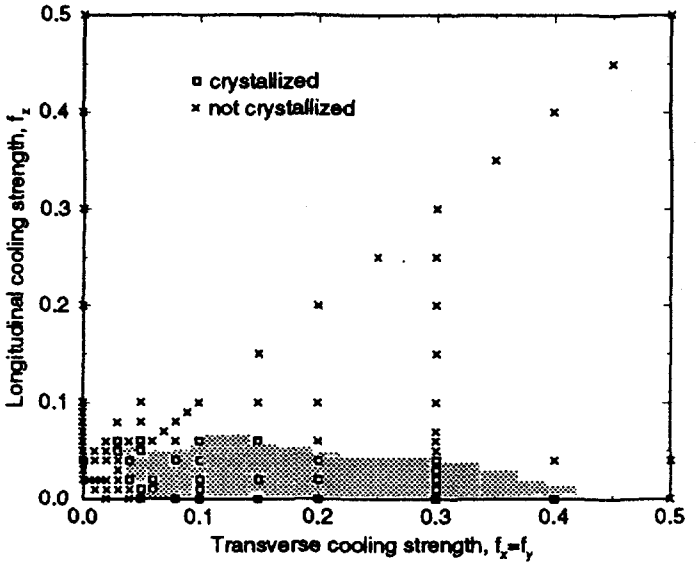

Figure 4: Beam crystallization by reducing the transverse (with $f_x = f_y$) and longitudinal (linear) momentum deviation. The shaded area and the squares indicate the region of cooling strengths with which the beam is successfully crystallized.

beam cooling, as previously discussed widely, is to impose a condition of longitudinal momentum (or velocity) variation with respect to the radial displacement (tapered cooling). We simulate this method by varying once per lattice period the longitudinal momentum P_z of each particle according to

$$\Delta P_z = -f_z \left(\dot{P}_i - C_{xz} x \right), \tag{17}$$

where, at the final stage of cooling when the temperature is extremely low ($T \leq 0.1$), we often assume $f_z = 1$. In the example of single-shell ground state (Section 5.1), the ordering can be achieved when the coefficient C_{xz} is within about $\pm 5\%$ of the ideal ground-state value ($C_{xz} \approx 0.285$).

6. Two-Species Crystals

Different species of charged ion beams travelling together with the same velocity will exchange energy via Coulomb interaction. The beam with lower temperature will absorb thermal energy from the beam with higher temperature. If cooling is applied on one ion species, the other ion species, with its temperature reduced, will be cooled "sympathetically".

In this section, we consider two species of ion beams with similar charge-to-mass ratio (Z/M) and similar rigidity, stored in the same storage ring. As we cool one species of ions, the total temperature of the two-species system decreases and, eventually, a crystalline state can be reached. As an illustrative example, we study the

system of equal density Ar^+ ($Z = 1$, $A = 39.9624$) and Se^{2+} ($Z = 2$, $A = 79.9225$) ions. The machine consists of 10 FODO cells with 25% bending with $\nu_x = 2.8$, $\nu_y = 2.1$. The bending radius is $\rho = 1$ m, and the average machine radius is $R = 4$ m. The beam energy is $\gamma = 1.00001$. The characteristic distance is $\xi = 1.2 \times 10^{-5}$ m.

Only the Ar^+ beam is externally cooled by imposing the periodicity condition in three directions (Section 5). Figs. 5 and 6 show the beam structure during the

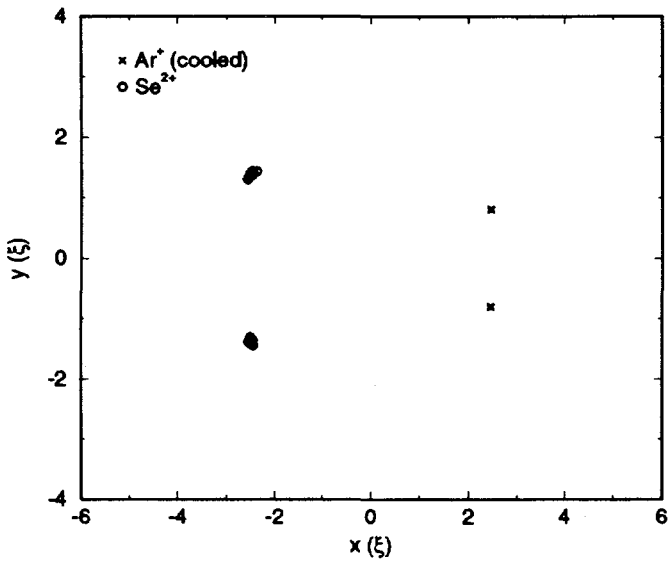

Figure 5: A two-species crystalline structure formed by Ar^+ ($A = 39.9624$) and Se^{2+} ($A = 79.9225$) ion beams of equal density ($N(Ar^+)/L = N(Se^{2+})/L = 0.5$, $L = 40\xi$) projected into the $x-y$ plane. Only Ar^+ beam is externally cooled. The temperatures are $T(Ar^+) = 5 \times 10^{-6}$, and $T(Se^{2+}) = 3 \times 10^{-4}$, respectively.

cooling process (after 100 revolutions of cooling on Ar^+) when the temperature of the Ar^+ beam is reduced to $T = 5 \times 10^{-6}$, and the temperature of the Se^{2+} beam is reduced sympathetically to $T = 3 \times 10^{-4}$. The crystalline state is stable when the external cooling is removed.

Due to the different charge-to-mass ratio Z/M between the different ion species, the average radial positions of the two beams are different. From Eq. 2, it can be estimated that the distance between the average radial beam centers x_c is

$$\Delta(x_c) \sim -\Delta\left(\frac{\bar{Z}}{m}\right) \frac{\rho}{\xi}, \tag{18}$$

i.e., it is linearly proportional to the difference in charge-to-mass ratio, and to the ratio ρ/ξ between the bending radius of the dipole magnets and the characteristic distance ξ. In Fig. 5, the positions of the Ar^+ ions are radially more outward from the center of the machine because of their relatively smaller Z/M.

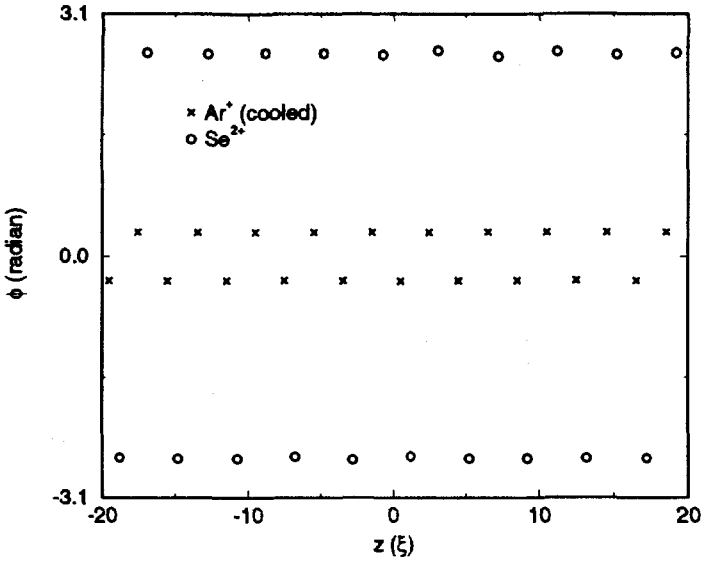

Figure 6: The same crystalline structure as shown in Fig. 5 projected into the $z - \phi$ plane, where ϕ is the polar angle.

7. Longitudinally Bunched "Crystal Balls"

We longitudinally bunch the beam of charged particles using rf cavities, located at one or more positions in the azimuth, with the rf electric voltage varying sinusoidally with time,

$$V(t) = V_0 \sin(h\omega_0 t), \tag{19}$$

where V_0 is the peak voltage, $\omega_0 \equiv \beta c/R$ is the revolution frequency of the reference particle, and h is the cavity harmonic number. Relative to the reference particle ($x = y = z = 0$), a particle of positive (or negative) z arrives at the cavity at a later (or earlier) phase and, therefore, experiences an energy gain per cavity:

$$eV_s = e\int E_s ds = eV_0 \sin\left(\frac{h\xi}{\gamma R}\, z\right). \tag{20}$$

In order to simulate the effect of a rf cavity, we employ Eq. 6 with $F_s = 0$ except in the region of the rf cavity. Because the cavity is a small fraction of the circumference, its effect can be approximated in a single numerical step using Eq. 20.

We find from the MD numerical studies that an rf field is no impediment to the formation of crystalline beams. Clearly, the rf field produces longitudinal bunching. Hence, the crystalline structures are finite in extent in all three directions. Among the many cases (1D, 2D, and 3D structures) that we have explored, we give one example in the series of figures from Fig. 7 to 11. The machine, having a periodicity of 10, consists of 10 FODO cells with 25% bending with $\nu_x = 3.1$, $\nu_y = 1.6$, and $\gamma_T = 2.9$. The beam energy corresponds to $\gamma = 1.4$. The rf voltage per lattice period

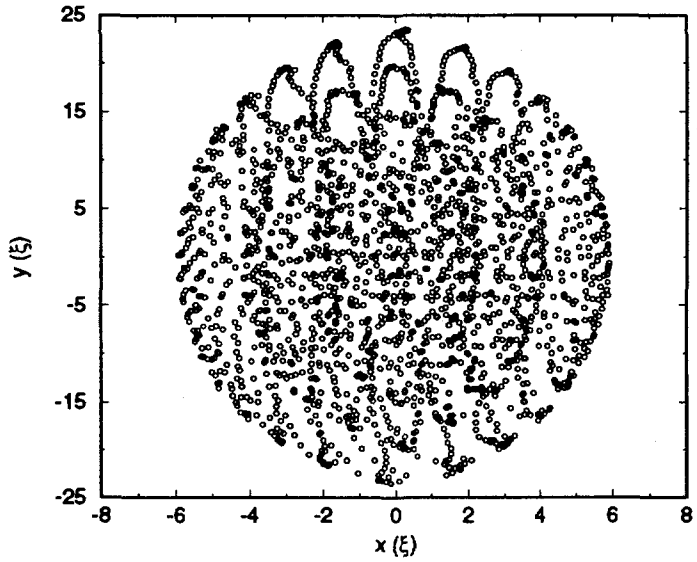

Figure 7: A multi-shell "crystal ball" structure with particle positions projected into the $x - y$ plane. Note that the structure is bunched in all three directions. The normalized temperature is $T \approx 2 \times 10^{-10}$.

is $V_0 = 200$ V. The machine parameters are chosen such that $\pi\gamma R/h\xi = 1000$, i.e., one rf wavelength corresponds to a distance from -1000ξ to 1000ξ (e.g. for $^{24}Mg^{2+}$ beam, $\xi = 6.4 \times 10^{-7}$; if $\rho = 1$ m, $R = 4$ m, then $h = 2.7 \times 10^4$.).

Fig. 7 shows a projection of the multi-shell structure into the transverse plane. In this example, $N = 2000$ particles are used for simulation. The structure is obtained by cooling (imposing the periodicity condition) the beam for 2,000 lattice periods (40,000 numerical steps). Figs. 8 and 9 show projections of the same structure into the $x - z$ and $y - z$ planes, respectively. Since one rf wavelength corresponds to a distance from -1000ξ to 1000ξ, this crystalline structure extends over about 1/10 of the rf period. The tilt in the $x - z$ plane in Fig. 8 is a result of the particular azimuthal location relative to the rf cavity at which the projection is made. Of course, the crystalline beam breathes and shears as it moves along the FODO lattice. The trajectories of positions and momenta are displayed for one out of the 2000 particles in Figs. 10 and 11, respectively. The rapid change in P_z in Fig. 11 is caused by the energy gain at the rf cavity.

The structure shown in Fig. 7 corresponds to a low temperature state of $T \approx 2 \times 10^{-10}$. After the cooling is turned off, the structure essentially remains unchanged. Further studies indicate that the heating rate for this bunched crystalline beam is similar to that for the un-bunched beam (Fig. 3).

With given beam and machine parameters and cavity h, the peak voltage V_0 determines the strength of the longitudinal focusing and, therefore, the longitudinal

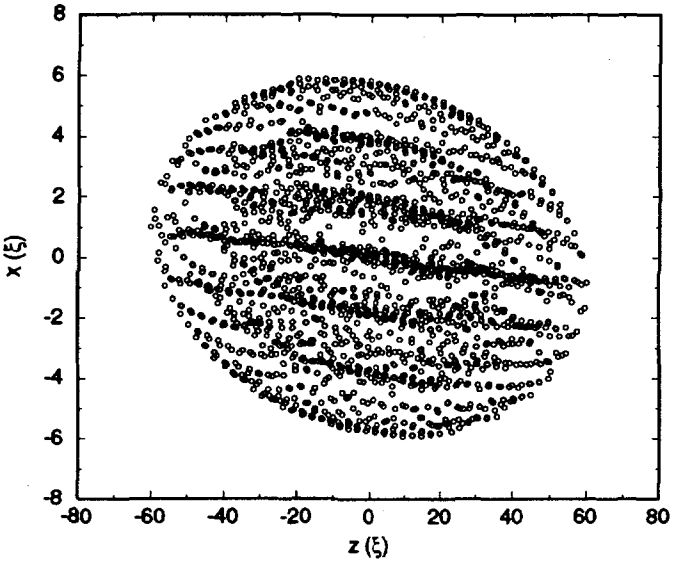

Figure 8: The same multi-shell structure as shown in Fig. 7 with particle positions projected into the $x - z$ plane.

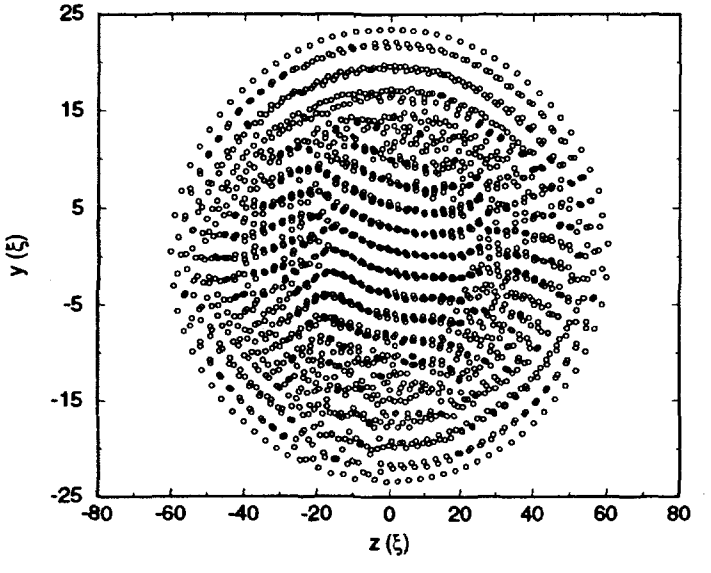

Figure 9: The same multi-shell structure as shown in Fig. 7 with particle positions projected into the $y - z$ plane.

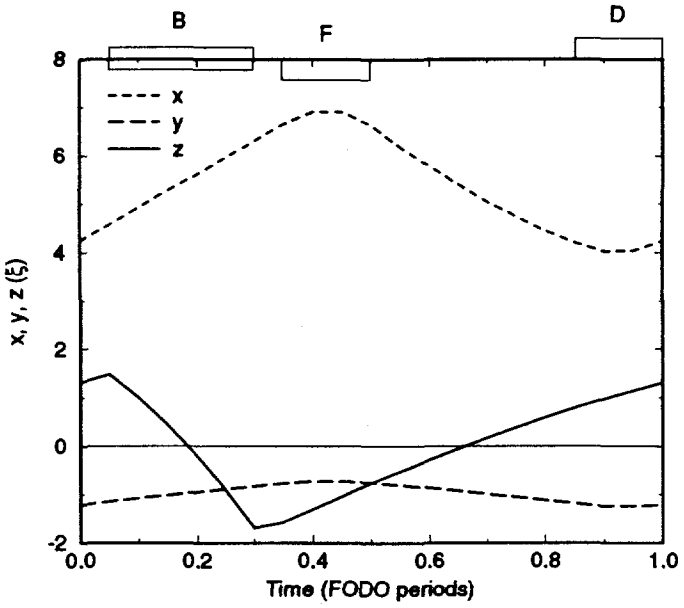

Figure 10: Typical particle trajectory of a bunched crystalline beam. Lattice components are displayed on the figure: B is a bending section, F and D are focusing and de-focusing sections.

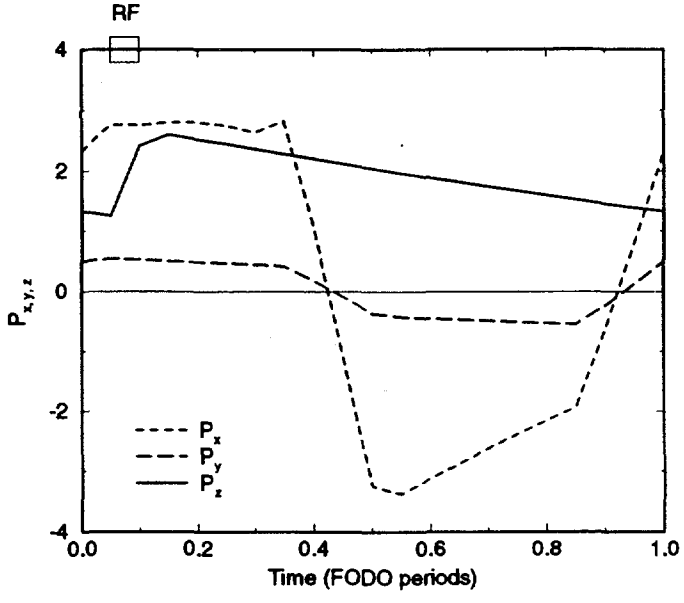

Figure 11: Typical particle momentum trajectory of a bunched crystalline beam. The location of the rf cavity is displayed on the figure.

size of the crystal. A higher (or lower) voltage results in a shorter (or longer) crystal length and higher (or lower) density in the longitudinal direction. Since the transverse intra-particle distance is mainly determine by the strength of the transverse focusing and the Coulomb force, this higher (or lower) longitudinal density results in a larger (or smaller) transverse crystal size. Obviously, if the voltage is sufficiently small, the crystal becomes de-bunched.

With given machine and rf cavity parameters, the nature of the crystalline ground state depends upon the number of particles confined in the distance of one rf wavelength (i.e. beam density). When the number of particles is small, the ground state is a 1D chain of finite length with smaller intra-particle distance for particles near the chain center. This chain tilts along x direction in the $x-z$ plane due to the energy increment caused by the rf cavity. As the beam density increases, the ground state becomes 2D extending in the plane of weaker transverse focusing. As the density increases further, the ground state becomes single and then multi-shell 3D, as shown in Figs. 7 - 9. The intra-particle distance, which is mainly determined by the strength of focusing and Coulomb force, is independent of the beam density. The conditions for the formation and maintenance of crystalline beams as discussed in Section 4 also apply to the bunched beam.

8. NAP-M Simulations

Having developed the formalism which allows us to study both highly developed and incipient crystalline beam structures, we are in a position to study, theoretically, the experimental situation on the NAP-M ring when it was used to study crystal formation in the late 1970's.[25]-[28] Actually in the experiment, the physicists were simply using electron cooling to reach the lowest possible temperatures. Compared with the un-cooled beam, the Schottky noise power for the cooled beam is reduced by approximately two orders of magnitude. Typically, the Schottky power decreases with the decreasing beam intensity. However, when the beam intensity is below $N_0 = 2\times10^7$, the Schottky power becomes independent of the intensity, corresponding to a longitudinal beam temperature of $T_{Bz} = 1$ K. It has later[28] been estimated that a crystalline state could have been observed at NAP-M at low intensity of $N_0 < 10^6$, outside of the range of the original measurement. At that time, no detailed theoretical analysis was performed; now, we are in a position to do just that.

We obtained the description of the NAP-M lattice and beam parameters primarily by private communication with Nicoli Dikanskiĭ. The machine circumference was 47.25 m, the lattice periodicity was 4, the transverse tunes were $\nu_x = 1.35$ and $\nu_y = 1.26$, the transition energy corresponded to $\gamma_T = 1.18$, and the beam energy corresponded to $\gamma = 1.07$. Electron cooling was employed to reduce the beam temperature. The lowest achieved temperatures were transverse T_{Bx}, $T_{By} = 50 \sim 100$ K, and longitudinal $T_{Bz} = 1$ K.

Using these parameters, we perform MD simulations in which electron cooling is simulated by reducing the momenta in three directions. Numerically starting from a high-temperature state, we turn off the cooling when the temperature falls into the desired range. Within the range of the experimentally measured beam intensity (from

$N_0 = 2 \times 10^6$ to 10^8), our MD simulation indicates no crystalline structure.

In order to verify Dikanskiĭ's speculation[28] that a crystalline state could have been observed at NAP-M at low intensity of $N_0 < 10^6$, we perform detailed study at the intensity of $N_0 = 1.5 \times 10^5$, outside of the range of the original experimental measurement. Fig. 12 shows the density of the beam as a function of radial distance ρ,

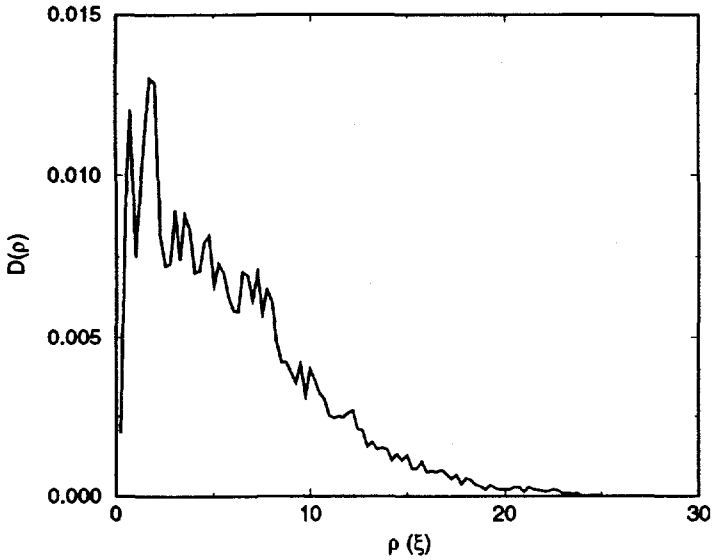

Figure 12: Density as a function of the radial distance ρ for the NAP-M simulation with $T_{Bx} \approx T_{By} \approx 50$ K, and $T_{Bz} = 1$ K, averaged over 22 μs and assuming $N_0 = 1.5 \times 10^5$. The radius ρ is measured in units of $\xi = 4.6\mu$m.

obtained using 40 particles per MD cell averaging over 50 revolutions (or a time period of 22 μs). The beam extends transversely to about 20ξ, or 0.11 mm. Fig. 13 shows the density of the beam as a function of longitudinal distance z, again averaging over 50 revolutions. Due to the relatively low beam intensity and relatively high transverse temperature, the beam behaves like a 1D chain of "disks" formed by transversely oscillating particles. Because of the non-zero longitudinal momentum spread (P_z) or temperature (T_{Bz}), the disks drift in the longitudinal direction, occasionally passing each other for lack of IBS interaction at low particle density.

In order to quantitatively determine the amount of longitudinal drift, we define the one-body correlation function $G_z(\tau)$,

$$G_z(\tau) = \langle (z_i(t+\tau) - z_i(t))^2 \rangle_{i,t}, \tag{21}$$

where $\langle\ \rangle$ denotes the average over all the particles i and over time t. Fig. 14 shows $G_z(\tau)$ as a function of time interval τ at three different longitudinal temperatures $T_{Bz} = 10$ K, 1 K, and 0.1 K, respectively, while the transverse temperatures are

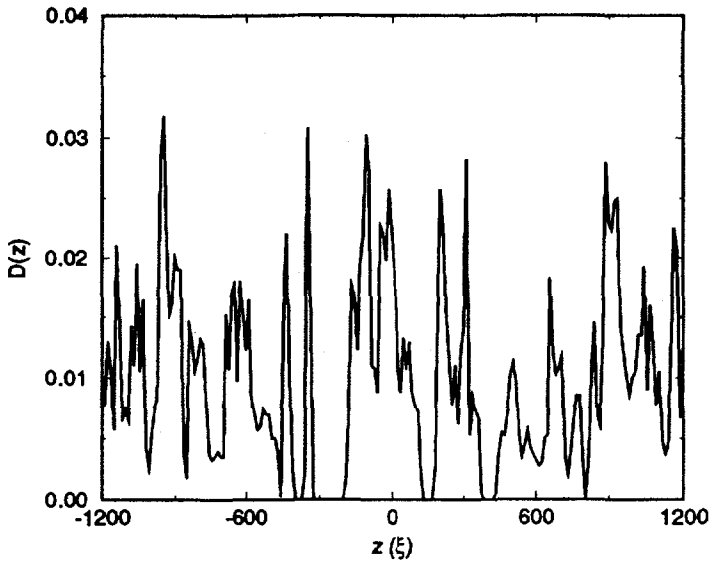

Figure 13: Density as a function of the longitudinal distance z for the NAP-M simulation with $T_{Bx} \approx T_{By} \approx 50$ K, and $T_{Bz} = 1$ K, averaged over 22 μs and assuming $N_0 = 1.5 \times 10^5$. The distance z is measured in units of $\xi = 4.6\mu$m.

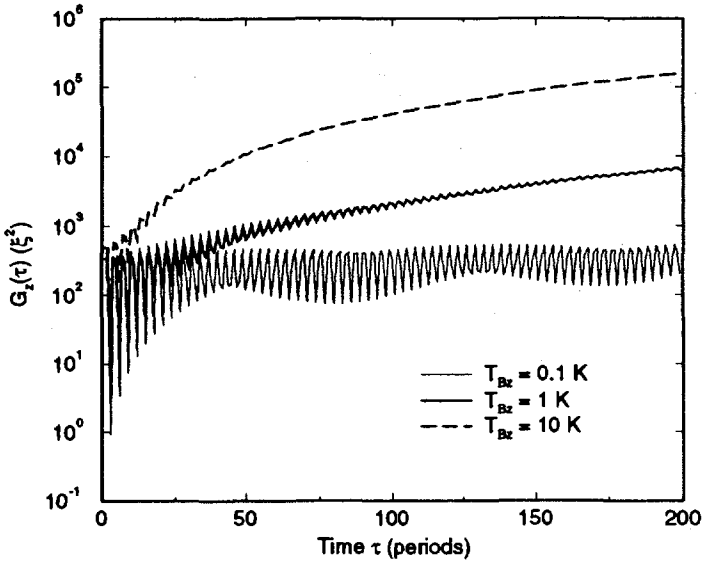

Figure 14: Longitudinal correlation functions as functions of time interval τ for the NAP-M simulations assuming $N_0 = 1.5 \times 10^5$. In the three cases shown, $T_{Bx} \approx T_{By} \approx$ 50 K, and $T_{Bz} = 10$ K, 1 K, and 0.1 K, respectively.

kept constant at $T_{Bx} \approx T_{By} \approx 50$ K (note the logarithmic scale). The zig-zag along each curve, with their amplitude proportional to the transverse temperature and their frequency the same as the horizontal betatron tune ν_x, is caused by the coupling between longitudinal (z) and horizontal (x) motion. At low temperature $T_{Bz} < 0.1$ K, G_z is approximately a constant in τ, and the disks are "frozen" in their longitudinal positions during the time of observation. At intermediate temperature $T_{Bz} \sim 1$ K, G_z increases linearly with τ, and disks drift and occasionally pass each other. In both cases, the longitudinal motion of the particles is much restricted, and the longitudinal Schottky signal will be greatly suppressed as observed experimentally. At high temperature, i.e. $T_{Bz} > 10$ K, the Coulomb interaction becomes negligible, and G_z is proportional to τ^2 in this gaseous state.

As long as the particle density is low so that the amplitude of the coupled z oscillation (which is of the same order as the transverse amplitude when T_{Bz} is much smaller than $T_{Bx,y}$) is much smaller than the longitudinal intra-particle distance, the rate of longitudinal drift is insensitive to the transverse temperature and beam intensity. When the particle density is high so that the amplitude in z is larger than the intra-particle distance, the disk structure no longer exists due to the large Coulomb interaction. In this case, the beam behavior can be described by the conventional IBS theory as discussed in Section 3.3.

9. New ASTRID Simulations

Detailed study of crystalline beams in the present ASTRID ring was presented in Ref. [21]. There, we have shown that only 1D structures were stable, and that 1D structures can only be achieved when the number of particles in the ring is less than 3.4×10^5. Furthermore, the maximum heating rate for the 100 keV $^7Li^+$ beam was shown to be $\Delta T/T \approx 4 \times 10^{-2}$ per lattice period, which corresponds to the minimum cooling rate needed for the crystal formation of 8×10^3 (K/sec) at the temperature of 1.5 K.

Even without developing a 1D crystal due to the high transverse temperature, one can develop an incipient crystal, analogous to what could have been observed at NAP-M at low beam intensity. Based on the machine parameters given in Ref. [21], we have performed numerical simulations similar to those for NAP-M. Assume that the transverse temperature is about 10^3 K. In order to form longitudinally well separated "disks", the number of particles in the ring should be less than about 3×10^4. On the other hand, the currently achievable longitudinal temperature of 1 mK is sufficiently low to keep the disks "frozen" in their longitudinal positions.

In the present ASTRID ring, 2D and 3D crystalline structures can not be maintained because the second condition (Section 4.2) is not satisfied. As a consequence, consideration is given to a proposed New ASTRID ring which satisfies both necessary conditions for the formation and maintenance of crystalline beams. According to the machine lattice obtained from Jeffrey Hangst, this machine has a periodicity of 4, and a circumference of 48.6 m. The transverse tunes are $\nu_x = 1.38$ and $\nu_y = 1.32$, and $\gamma_T = 1.29$. The beam energy is $\gamma = 1.000016$. Not surprisingly, ground states of all dimensions can be readily achieved. An example of a 3D state is given in Fig. 15.

The heating rates obtained for 1D, 2D, and 3D crystalline states are similar to those

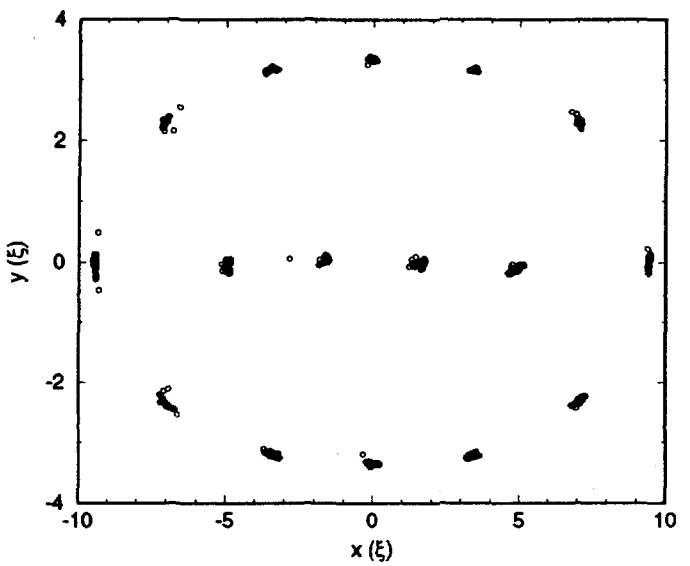

Figure 15: A 3D structure with particle positions projected into the $x-y$ plane. The New ASTRID ring has a periodicity of 4 with $\nu_x = 1.38$, $\nu_y = 1.32$. The beam energy is $\gamma = 1.000016$. The calculation is done with $N = 400$, and $L = 100\xi$.

shown in Fig. 3.

Numerical studies were made also for the case of $\nu_x = 1.67$ and $\nu_y = 1.68$. Since the second condition was in this case violated, it was again not surprising to find that only 1D crystals could be formed and maintained, as shown in Fig. 16.

10. Conclusions

We have presented the equations of motion appropriate to interacting charged particles of diverse charge and mass, subject to the external forces produced by bending dipole, AG focusing quadrupole, and sextupole magnets, and by bunching rf cavities in real storage rings. Employing these equations in the molecular dynamics simulations, we obtained heating rates of the crystalline beam as functions of beam density and temperature. In the high temperature limit, it has been shown that the MD results agree well with the intra-beam scattering theory.

As presented in our previous papers, there are two necessary conditions for the formation and maintenance of the crystalline beam. The first condition requires that the storage ring is AG focusing operating below the transition energy. The second condition requires that the lattice periodicity of the ring is at least $2\sqrt{2}$ as high as the maximum betatron frequency tune.

Various cooling methods have been studied using the MD simulation. Provided that the cooling rate is adequate, the present cooling techniques suffice in making 1D

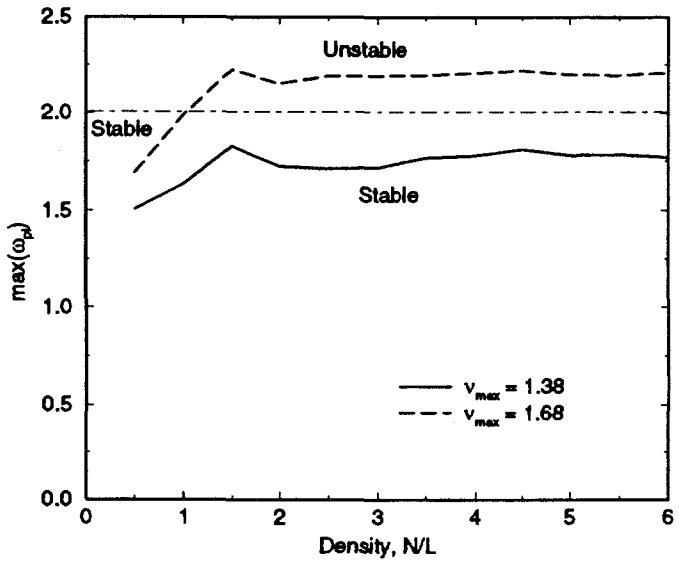

Figure 16: The maximum phonon frequencies as functions of beam density at various design transverse tunes. The crystalline structure is unstable when the maximum phonon frequency is higher than half of the lattice frequency. Here, the lattice periodicity is 4.

crystals. In order to achieve higher-density ordered states, it is necessary to develop cooling methods that are more effective in the transverse direction.

The formalism has been used to study the formation of crystalline beams of two different ion species of similar charge-to-mass ratio. It is shown that cooling only one of the two species can result in a crystalline state of both species; i.e., that the mutual interaction of the particles leads to sympathetic cooling.

The formalism has also been used to study the effect of rf fields upon a bunch of charged particles. It is shown that "crystal balls" with finite extent in all three directions can be formed and maintained.

We have studied the NAP-M ring where anomalous Schottky behavior was observed. Using the tools that we have developed, we reconstruct the conditions of the NAP-M experiment. It is found that no crystalline state can be reached at the original experimental range of beam intensity and temperature. On the other hand, at extremely low beam intensities, an incipient crystalline structure could be observed at the NAP-M installation with the particles forming into occasionally-passing disks.

Finally, we have studied the New ASTRID ring which has been proposed for the formation and study of crystalline beams. Note that the existing rings in Denmark and Germany do not satisfy the second necessary condition and, consequently, would only allow the formation of 1D structures. It is shown that the New ASTRID ring would be suitable for the formation of crystalline beams of all dimensions.

In summary, we have shown that the formalism and numerical methods that

we have developed allow one to study a diversity of topics in crystalline beams. Such subject seems rich, indeed, and one eagerly awaits experimental realization of crystalline beams.

Acknowledgements

The authors would like to thank J. Hangst, D. Habs, N.S. Dikanskiĭ, and I. Hofmann for useful discussions, and D. Reistad for pointing out an error in our assumption of the NAP-M experimental condition.

References

[1] N.S. Dikanskiĭ and D.V. Pestrikov, Proc. of the Workshop on Electron Cooling and Related Applications, KfK 3846, ed. H. Poth, (1984).

[2] J.P. Schiffer and P. Kienle, Z. Phys. A **321**, 181 (1985).

[3] J.P. Schiffer and O. Poulsen, Europhys. Lett. **1**, 55 (1986).

[4] A. Rahman and J.P. Schiffer, Phys. Rev. Lett. **57**, 1133 (1986).

[5] D. Habs, MPI Heidelberg preprint MPIH-1987-V10 (1987).

[6] J.P. Schiffer, Phys. Rev. Lett. **61**, 1843 (1988).

[7] R.W. Hasse and J.P. Schiffer, Ann. Phys. **203**, 419 (1990).

[8] R.W. Hasse, GSI preprint GSI-90-23 (1990).

[9] R.W. Hasse and V.V. Avilov, Phys. Rev. A **44**, 4506 (1991).

[10] J.P. Schiffer, Phys. Rev. Lett. **70**, 818 (1993).

[11] J.P. Schiffer and A. Rahman, Z. Phys.A – Atomic Nuclei 331, 71–74 (1988).

[12] J.P. Schiffer, Proc. of the Workshop on Crystalline Ion Beams, Werheim, Germany, 2 (1988), ed. R.W. Hasse, I. Hofmann, D. Liesen.

[13] J.P. Schiffer and A. Rahman, Z. Phys.A-Atomic Nuclei **331**, 71 (1988).

[14] J.P. Schiffer, Proc. of the Workshop on Crystalline Ion Beams, Werheim, Germany, editors R.W. Hasse, I. Hofmann, and D. Liesen, p.2 (1988).

[15] J. Beebe-Wang, N. Elander and R. Schuch, Nucl. Instrum. Methods **B79**, 806 (1993).

[16] J. Wei, X-P Li, and A.M. Sessler, "Crystalline Beam Ground State", Brookhaven National Laboratory Report BNL-52381, Upton, New York (1993).

[17] J. Wei, X-P Li, and A.M. Sessler, "Crystalline Beam Ground State", Proc. of The 1993 Particle Accelerator Conference,Washington, May 1993, p. 3527.

[18] J. Wei, X-P Li, and A.M. Sessler, "Critical Temperatures for Crystalline Beams", Proc. of the Workshop on Beam Cooling and Related Topics, Montreux, October 1993, p. 366.

[19] J. Wei, X-P Li, and A.M. Sessler, "The Low-Energy States of Circulating Stored Ion Beams: Crystalline Beams", Physical Review Letters **73**, 3089 (1994).

[20] J. Wei, X-P Li, and A.M. Sessler, "Crystalline Beams", Advanced Accelerator Concepts, Fontana, June 1994, AIP Conference Proceedings **335**, ed. P. Schoessow, p.224, (1995).

[21] J. Wei, X-P Li, and A.M. Sessler, "Crystalline Beam Properties as Predicted for the Storage Rings ASTRID and TSR", Proc. of the 1995 Particle Accelerator Conference, Dallas, 1995 (to be published). Note that the 2D ground state that we found for the TSR ring rotates once per lattice period along its longitudinal axis. Further study of the structure has shown that the rotation can be either clockwise or counter-clockwise, i.e., the two rotation states are degenerate.

[22] X-P Li, A.M. Sessler, and J. Wei, "Crystalline Beams in a Storage Ring: How Long Can It Last", Proc. of the 1994 European Particle Accelerator Conference, London, 1379 (1994).

[23] J. Wei, "Evolution of Hadron Beams under Intrabeam Scattering", Proc. 1993 Part. Accel. Conf. Washington D.C., p.3651 (1993).

[24] J. S. Hangst, *Laser Cooling of a Stored Ion Beam - A First Step Towards Crystalline Beams*, Ph.D Thesis, 1992, Argonne National Laboratory Report ANL/PHY-93/1.

[25] V.V. Parkhomchuk and N.S. Dikanskiĭ, Sov. Journ. of Tech. Phys., bf 50, 1411 (1980).

[26] E.E. Dement'ev, N.S. Dikanskiĭ, A.S. Medvedko, V.V. Parkhomchuk and D.V. Pestrikov, Zh. Tekh. Fiz **50**, 1717 (1980); English transl. Sov. Phys. Tech. Phys. **50**, 1001 (1980).

[27] V.V. Parkhomchuk and A.H. Skrinsky, Report on Progress in Physics, bf 54, 919 (1991).

[28] N.S. Dikanskiĭ and D.V. Pestrikov, *The Physics of Intense Beams and Storage Rings*, AIP Press (1994).